Process modelling, design and technoeconomic evaluation for continuous paracetamol crystallisation

Process modelling, design and technoeconomic evaluation for continuous paracetamol crystallisation

Hikaru Jolliffe and Dimitrios I. Gerogiorgis*

Institute for Materials and Processes (IMP), School of Engineering, University of Edinburgh, The King's Buildings, Edinburgh, EH9 3FB, United Kingdom

**Corresponding author: D.Gerogiorgis@ed.ac.uk (+44 131 6517072)*

ABSTRACT

Continuous Pharmaceutical Manufacturing (CPM) has a strong potential to catalyse pharmaceutical innovation. This paper analyses Continuous Oscillatory Baffled Crystalliser (COBC) optimal design and performance for paracetamol crystallisation, via systematic modelling and nonlinear optimization (NLP). Clear trends emerge, with rate of antisolvent use having a marked impact of COBC volumes; crystal seed mass loading also has a strong effect. For the base case studied (inlet temperature of 50 °C, seed crystal size of 40 microns) the optimal solution was for 2% seed mass loading (with respect to solute mass) and with 80% water antisolvent use (by mass with respect to process solvent acetone); the crystalliser size was 4.25 L with a total cost of 101,370 GBP, achieving a product yield of 50% with a product crystal size of 83.6 microns. Clear tradeoffs among mass efficiency, volume, cost and product crystal size have been illustrated, providing valuable quantitative insights into process performance.

1 INTRODUCTION

Pharmaceutical production has long relied solely on batch processing, and while it has many benefits including equipment flexibility and the know-how of a mature technology, in an environment of growing R&D expenditure (Fig. 1) and a greater awareness of and a drive to be more sustainable, research interest has turned towards Continuous Pharmaceutical Manufacturing (CPM); continuous production can achieve higher yields purities, better heat and mass transfer, decreased processing times, and better efficiency and reliability. The need for cost-effective R&D methodologies brings process modelling and simulation to the forefront of initial stages of process option evaluation. Furthermore, they are also of great utility in evaluating alternative design parameters for existing or newly developed processes (Benyahia et al., 2012). Continuous crystallisation has received significant research attention toward developing separation technologies for CPM, with both stirred tanks and tubular crystallisers studied (Ferguson et al., 2014; McGlone et al., 2015; Diab and Gerogiorgis, 2017). Achieving high product quality is also extremely important: accordingly, high-fidelity dynamic population balance models and algorithms have been employed to ensure precise control of the output Particle Size Distributions (PSD) via cooling and seeding (Shi et al., 2006; Kwon et al., 2014a-c).

In recent years the continuous synthesis of a range of APIs has been demonstrated, from common over-the-counter medications to key anti-cancer drugs (Bogdan et al., 2009; Hopkin et al., 2010). While there have been some significant advances with regards to complete ingredient-to-product demonstrations of CPM, many aspects of continuous product separation remain to be fully investigated (Heider et al., 2014; Baxendale et al., 2015).

The simulation and cost estimation of process models are invaluable methodologies for evaluating the benefits of continuous processing for the production of pharmaceuticals (Gerogiorgis and Barton, 2009; Rogers et al., 2014; Rogers and Ierapetritou, 2015; Jolliffe and Gerogiorgis, 2015-2017). The field of mathematical programming, commonly also called optimisation, has also been utilized to great effect, including for many aspects of pharmaceuticals and CPM (Biegler and Grossmann, 2004; Gernaey et al., 2012; Escotet-Espinoza et al., 2016).

Typical examples include the use of the Levenberg-Marquadt algorithm to significantly reduce the number of initial approximations required for global optimisation of Lorcaserin synthesis (Grom et al. 2016). Another example is the optimisation of a small-scale design for continuous ibuprofen synthesis (Patel et al., 2011), where in the latter example the objective was the minimisation of the difference between heat removed from and heat generated by the microreactor assembly; constraints and bounds included residence times, temperature, and concentrations.

Downstream processes, especially final product formulation, have also attracted significant

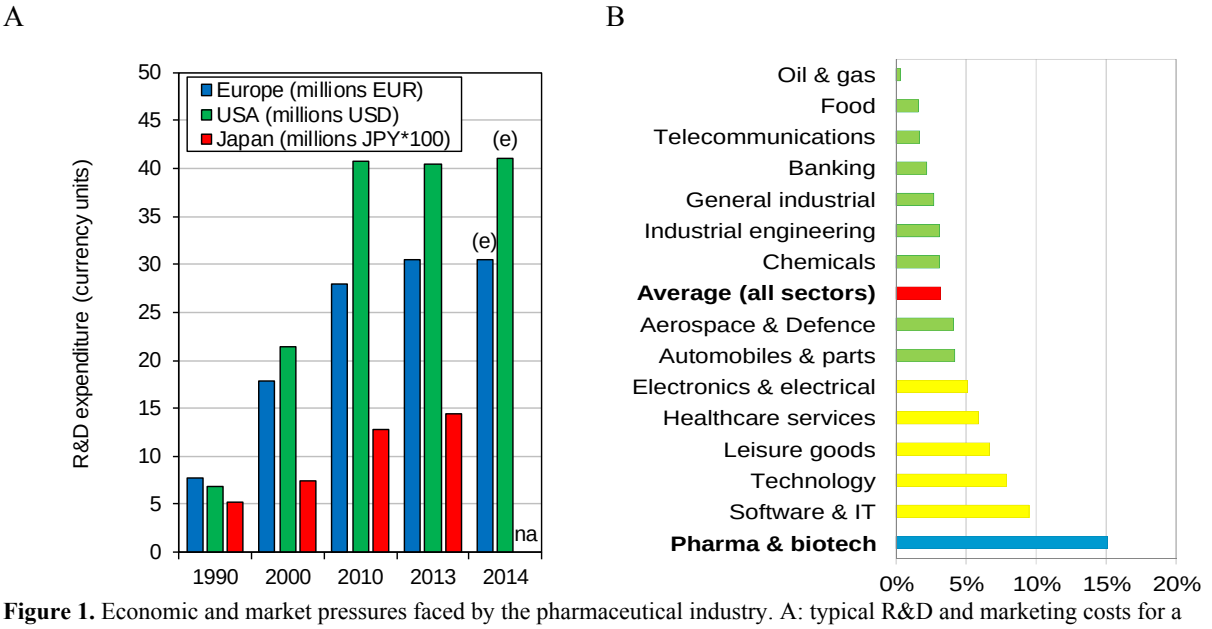

Figure 1. Economic and market pressures faced by the pharmaceutical industry. A: typical R&D and marketing costs for a high-volume, 'blockbuster' drug. B: varying sector R&D costs as a percentage of total sales. (EFPIA, 2013).

research interest in terms of optimisation (Boukouvala and Ierapetritou, 2013; Sen et al., 2013; Abejón et al., 2014; Sato et al., 2015). Key research areas include the use of surrogate-based optimisation to reduce the computational cost of complex solid-based flowsheet models (Boukouvala and Ierapetritou, 2013), the use of reduced-order models combined with population balance models in the explicit optimisation of downstream flowsheets using multiple objective functions for each unit operation (Sen et al., 2013), and the optimisation of novel technologies such as complex nanofiltration cascades (Abejón et al., 2014).

Life-cycle assessment optimisation is also an interesting aspect of optimisation applied to CPM. Ott and co-workers (2014, 2016) have elucidated how multiple rufinamide synthesis routes can be comparatively evaluated by the systematic consideration of technical and sustainability performance criteria such as Process Mass Intensity (PMI), the Environmental Factor (E-factor) and Life Cycle Impact Assessments (LCIA), with the latter being reduced by 45 % as a result.

In previous work, we have used modelling and simulation to economically evaluate two CPM processes, and we have also used nonlinear optimisation of these process models to determine optimal design and operating parameters for key product separation operations (Jolliffe and Gerogiorgis, 2017a, 2017b). In the present work, we systematically incorporate models for continuous crystallisation, published crystallisation kinetic data, and economic analysis into a nonlinear optimisation model to determine optimal crystallisation operation and design for the recovery of an analgaesic Active Pharmaceutical Ingredient (API), paracetamol. This key API has been widely used as a model API for CPM studies, with published data on crystallisation kinetics available (Brown et al., 2015; Cruz et al., 2016). The impact of temperature, crystalliser size and configuration, antisolvent type and quantity, and flowrate are considered. The optimisation cases are formulated into a nonlinear optimisation model to determine optimal Continuous Oscillatory Baffled Crystalliser design variables and process conditions. Technical metrics (such as product recovery), Green Chemistry metrics (E-factor), and economic metrics (Capital Expenditure, CapEx) are used for process evaluation.

1.1 Continuous Oscillatory Baffled Crystallisers (COBC)

Continuous Oscillatory Baffled Crystallisers (COBC) are a development resulting from Oscillatory Baffled Reactors: they comprise a series of baffles in long (i.e. high length-to-diameter ratio) tubes, and in appearance are similar to Plug Flow crystallisers with baffles. COBC units tend to offer improved performance over the latter, as well as over batch crystallisers. They offer improved scaling, heat and mass transfer and decreased processing times (Lawton et al., 2009). COBC units operate by inducing an oscillatory flow in the fluid contents, and there is also a net flow through the unit (as this is a continuous process) which is independent of the oscillatory flow. The use of a reciprocating pump is a common way to generate the oscillatory flow, and as the fluid moves back and forth across the baffles eddies are generated which enhance mixing and therefore performance. Baffles design primarily varies in terms of the orifice-to-internal diameter ratio, the gap between the baffles and the number of orifices in the baffles; in some cases constrictions are used instead of baffles (Fig. 2).

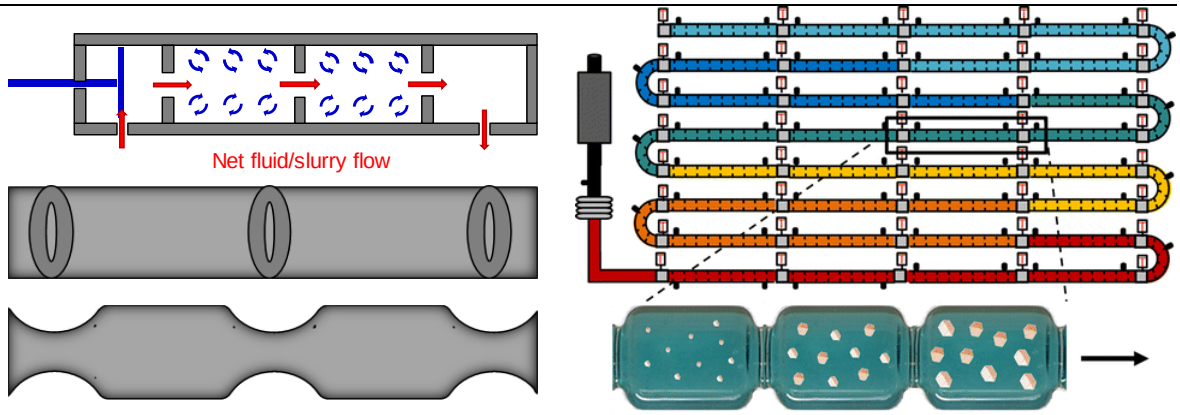

Figure 2. Typical examples of oscillatory baffled crystalliser design (Hodges, 2015; McGlone et al., 2015).

2 PROCESS MODEL AND NONLINEAR OPTIMISATION

The objective function to be minimized is a Capital Expenditure (*CapEx*) function (Equation 1), from a capacity-power law using crystalliser volume. The coefficient a and exponent n were generated by fitting publicly available data for cost and capacity of commercial COBC units. Crystalliser volume is computed in a relatively straightforward manner (Equation 2), from total volumetric throughput and the residence time required to achieve the desired objectives (such as yield). The population balance (Equation 3) and mass balance (Equation 4) are solved via a moment transformation (Equation 5) (Brown et al., 2014). Key variables in (Equation 5) include characteristic crystal length L (m), growth rate G (m s^{-1}).

There are two main forms which are encountered, forms I and II (Fig. 3). Form I is monoclinic and forms more readily, and Form II is orthorhombic and metastable. Indeed, active measures must often be taken to promote the formation of Form II. Here in this work, Form I is assumed, as the empirical correlations to estimate growth rate are based on experimental work where Form I was present; the volume shape factor k_v is taken to be 0.866 (Brown and Ni, 2011). Crystal density ρ_{API} is 1.3 g cm^{-3}.

Nucleation is considered to be negligible, so the Br_o^j terms in Equation (5) are ignored. Growth rate G is computed via an empirical correlation (Equation 6) (Brown and Ni, 2011), where ΔC_{API} is the degree of supersaturation (Equation 7), $\dot{Q}_{AS}$ is the rate of antisolvent addition in mL min^{-1}, and Re_o the oscillatory flow Reynold Number (Equation 9).

In the oscillatory flow Reynold Number, angular velocity $\omega = 2\pi f_{osc} a_{osc}$ (m s^{-1}) replaces the superficial fluid velocity found in the normal (Net Flow) Reynolds Number (Re_n, Equation 9). Here, f_{osc} and a_{osc} are the frequency and amplitude of the fluid oscillation, respectively (normally taken to be 2 Hz and 10 mm in this model). In the literature, values for both Re_o and Re_n are suggested to achieve the best mixing, often above 300 for the former and above 50 for the latter. In this model we have imposed similar requirements, although with a higher Re_o; values over 4,000 have been used in experimental work (Brown and Ni, 2011). There is also ψ, the ratio of Re_o and Re_n, and again the literature suggests a range for best mixing, which has been employed in this study. The ranges listed in Equation (9) are not hard constraints, and in some cases operation falls outside by 10%.

The solubility of paracetamol in different solvent systems has been commonly studied in the literature. Here, the use acetone as process solvent is modelled, with either water or toluene as antisolvent. Empirical values for paracetamol were taken fitted high order polynomial surrogate equations to calculate solubilities (Equation 8). With water use there is a solubility peak, and within a certain range adding water will in fact increase API solubility. To avoid this, the rate of antisolvent

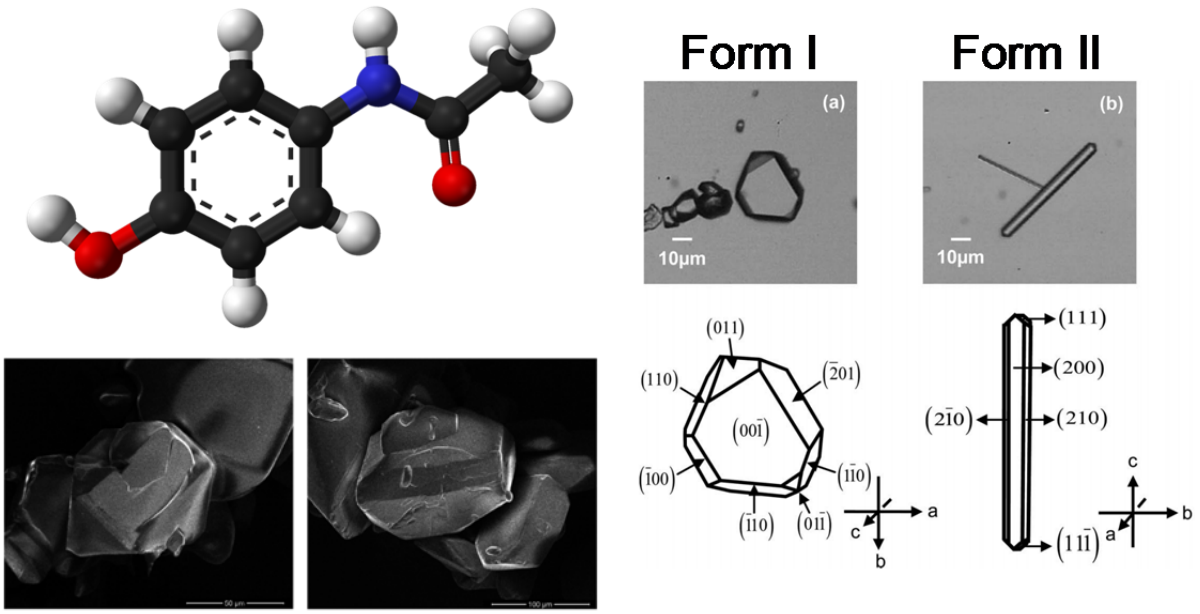

Figure 3. Paracetamol molecular structure and typical crystal polymorphs (Brown and Ni, 2011; Sudha and Srinivasan, 2013).

$$\min CapEx = aV_{COBC}{}^{m} \tag{1}$$

s.t.

$$V_{COBC} = \dot{Q}_{Tot}\tau_{req} \tag{2}$$

$$\frac{\delta n}{\delta t} + G\frac{\delta n}{\delta L} = 0 \tag{3}$$

$$\frac{\mathrm{d}C_{API}}{\mathrm{d}t} = -3\rho_{API}k_v G\int_0^{\infty} L^2 n\,\mathrm{d}L \tag{4}$$

$$\mu_j = \int_0^{\infty} L^j f_n(L,t)dL, \qquad \begin{bmatrix} \dot{\mu}_0 \\ \dot{\mu}_1 \\ \dot{\mu}_2 \\ \dot{\mu}_3 \\ \dot{\mu}_{C_{API}} \end{bmatrix} = \begin{bmatrix} B \\ G\mu_0 + Br_0 \\ 2G\mu_1 + Br_0^2 \\ 3G\mu_1 + Br_0^3 \\ -\rho_{API}k_v(3G\mu_1 + Br_0^3) \end{bmatrix} \tag{5}$$

$$G \cdot 10^8 = 3.78 \cdot 10^{-12}\Delta C_{API}^{1.570}\dot{Q}_{AS}^{1.158}Re_o^{2.155} + 21.50 \tag{6}$$

$$\Delta C_{API} = C_{API} - C_{API}^{sat},\ S = \frac{C_{API}}{C_{API}^{sat}} \tag{7}$$

$$C_{API}^{sat} = \sum_{i=0}^{n}\sum_{j=0}^{k} a_{ij} m_{AS,\%}{}^{i} T^{j} \tag{8}$$

$$Re_o = \frac{2\pi f_{osc} a_{osc}\rho_{mix} d}{\mu_{mix}} > 1000,\ Re_n = \frac{\rho_{mix} u_{net} d}{\mu_{mix}} > 40,\ 10 > \psi = \frac{Re_o}{Re_n} > 4 \tag{9}$$

$$0.5 \le ASR \le 0.8 \tag{10}$$

$$0.5\frac{kg_{seed}}{kg_{solvent}} \le 100SMR \le 2.0\frac{kg_{seed}}{kg_{solvent}} \tag{11}$$

use was limited to a range of 50:50 to 20:80 by weight (process solvent acetone : antisolvent). Because using toluene has been found to result in highly impractical residence times and volumes (very long/large); the results presented here refer to the use of water as an antisolvent.

Seed crystal loading can vary from 0.5% to 2.0% by weight (seed w.r.t. solvent and antisolvent). The following assumptions are made: a) seed crystals are monodisperse (i.e. of same size) and of monoclinic Form I; b) no nucleation, agglomeration or breakage of crystals; c) crystal growth rates are size-independent; d) no impurities; e) sufficient heat transfer available to maintain a linear cooling profile. In terms of temperature, the inlet temperature can vary between 30 to 70 °C, and cooled to 5 °C; an inlet temperature of 50 °C has been the default studied, with other values investigated to see how optimal points change. Likewise, seed crystal size was 40 microns by default, in order to ensure that the correlation used complies with literature (Brown and Ni, 2011); only crystal sizes equal to or higher than this threshold have been investigated, to study the variation of optima. Separate optimisation cases have been solved for varying inlet temperature and varying seed crystal size.

The solver employed is a constrained minimization solver using the trust region reflective algorithm, with tolerances (stopping criteria) set to 10^{-6}. Gradients were computed by the solver itself, and the solution time was reasonably fast at between 30–100 seconds; these values are the time required to generate capital expenditure response surfaces, and the time to run a single optimisation case was faster at 5–10 seconds. As stated, separate cases were formulated for initial temperatures. Separate cases were also performed for seed crystal sizes. A quick global search was performed by checking convergence from multiple initial starting points; the runs always converged to the same point, and the absence of local minima can be concluded with good confidence.

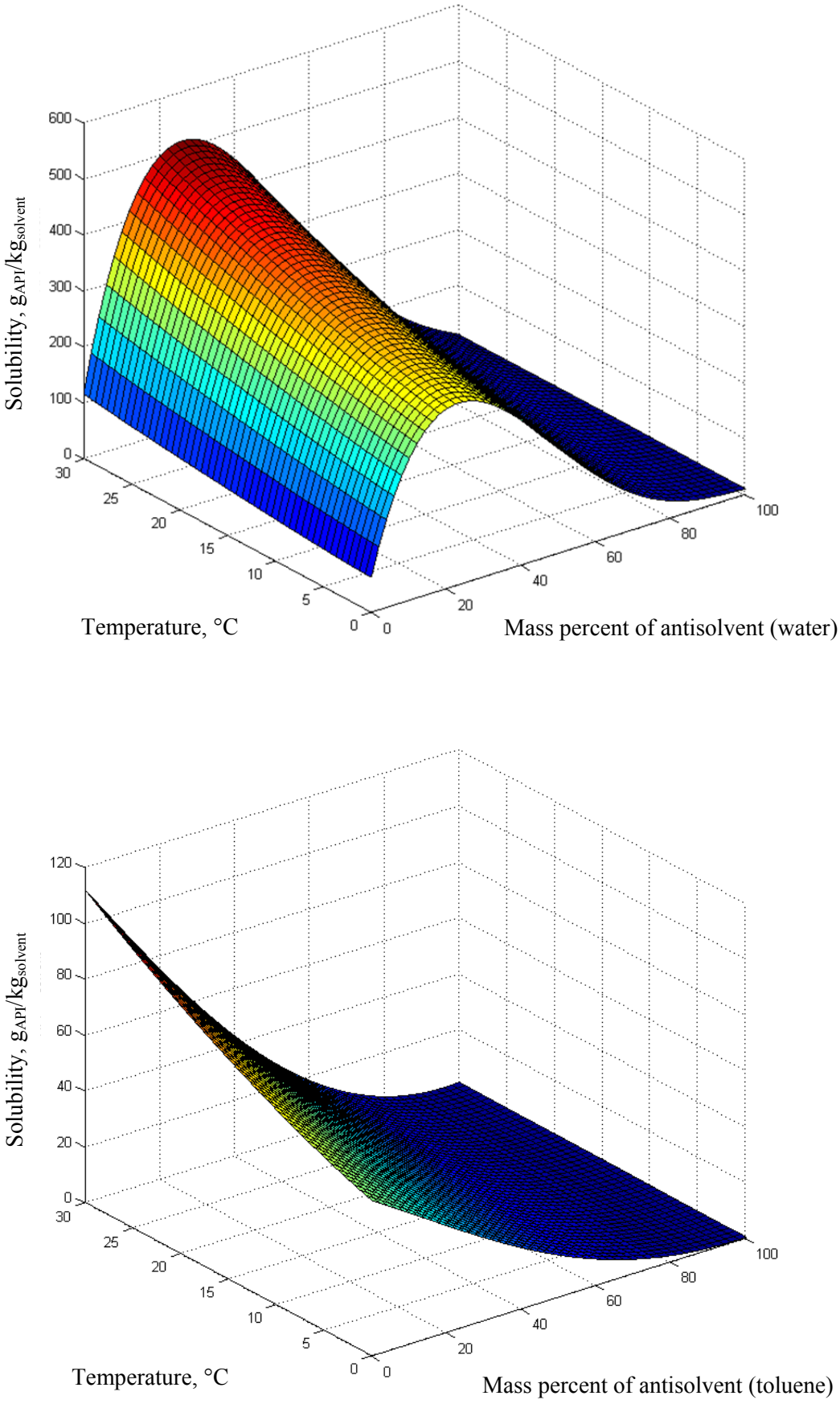

Figure 4. Paracetamol solubility in acetone-antisolvent mixtures (top = water antisolvent, bottom = toluene antisolvent).

Table 1. Optima variation for differing inlet temperatures (left) and seed crystal size (right).

Seed crystal size L_s = 40µm					*Inlet temperature* T_{in} = 50°C				
T_{in} (°C)	*CapEx* (10^3 £)	V_{COBC} (L)	τ_{req} (s)	L_p (µm)	L_s (µm)	*CapEx* (10^3 £)	V_{COBC} (L)	τ_{req} (s)	L_p (µm)
70	37.032	0.941	91	118.0	80	161.060	8.499	822	167. 2
60	60.337	1.954	189	99.2	70	147.280	7.435	719	146.3
50	101.370	4.250	411	83.6	60	132.970	6.380	617	125.4
40	170.600	9.265	896	71.5	50	117.700	5.315	514	104.5
30	283.530	19.822	1917	62.4	40	101.370	4.250	411	83.6

3 RESULTS AND DISCUSSION

3.1 Dynamic simulation of crystallisation evolution

Plotting the trajectories of some key variables shows the expected trends (Fig. 5). The yield takes time to develop, as the growth rate is initially slow. As time progresses (i.e. the material moves through the crystalliser), the supersaturation grows as the API precipitation does not keep pace with the decreasing solubility, the latter coming from the temperature decreasing in a linear manner). As the supersaturation – the gap between the blue solubility curve and the red concentration curve – increases, the growth rate begins to increase, naturally leading to an enhancement of the rate of yield increase. Eventually, the concentration lowers to the point where the trend reverses and the supersaturation begins to decrease, at which point there is an inflection in the yield trajectory, and the yield begins to trend towards a plateau.

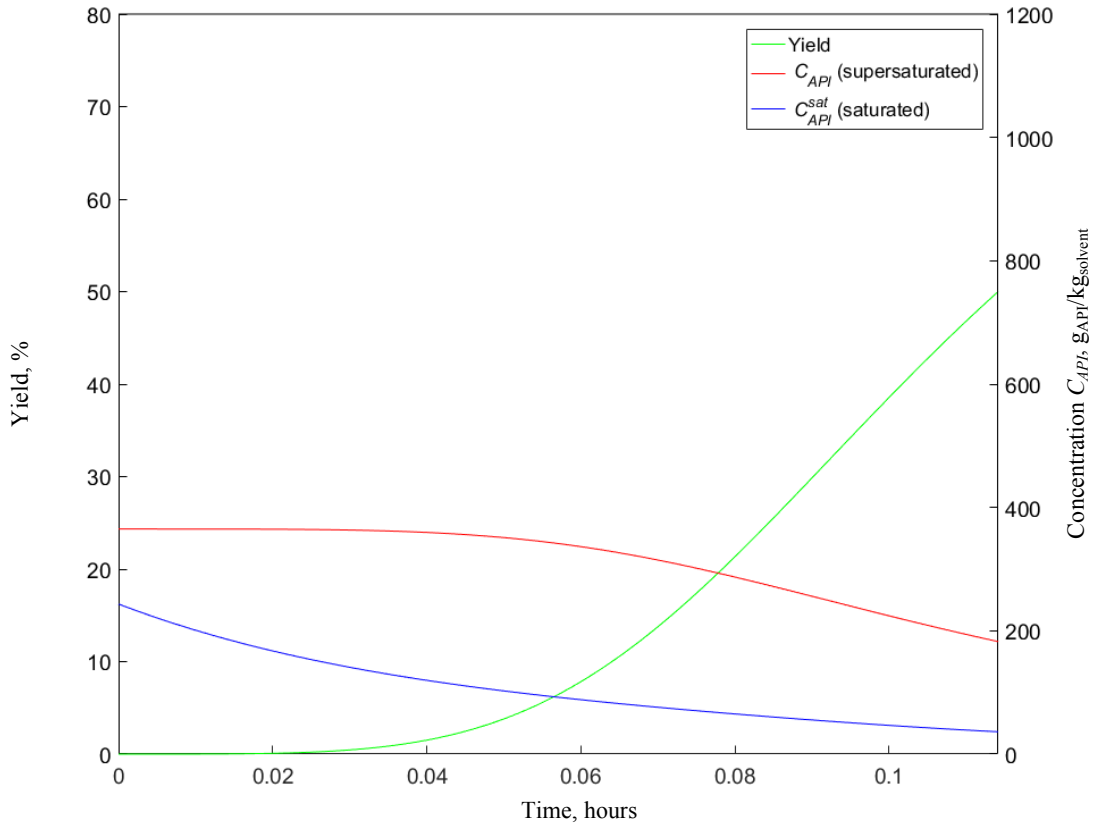

Figure 5. Trajectory of key process variables. The seed crystal size is 40 microns and the outlet temperature is 5 °C, and the inlet temperature is 50 °C.

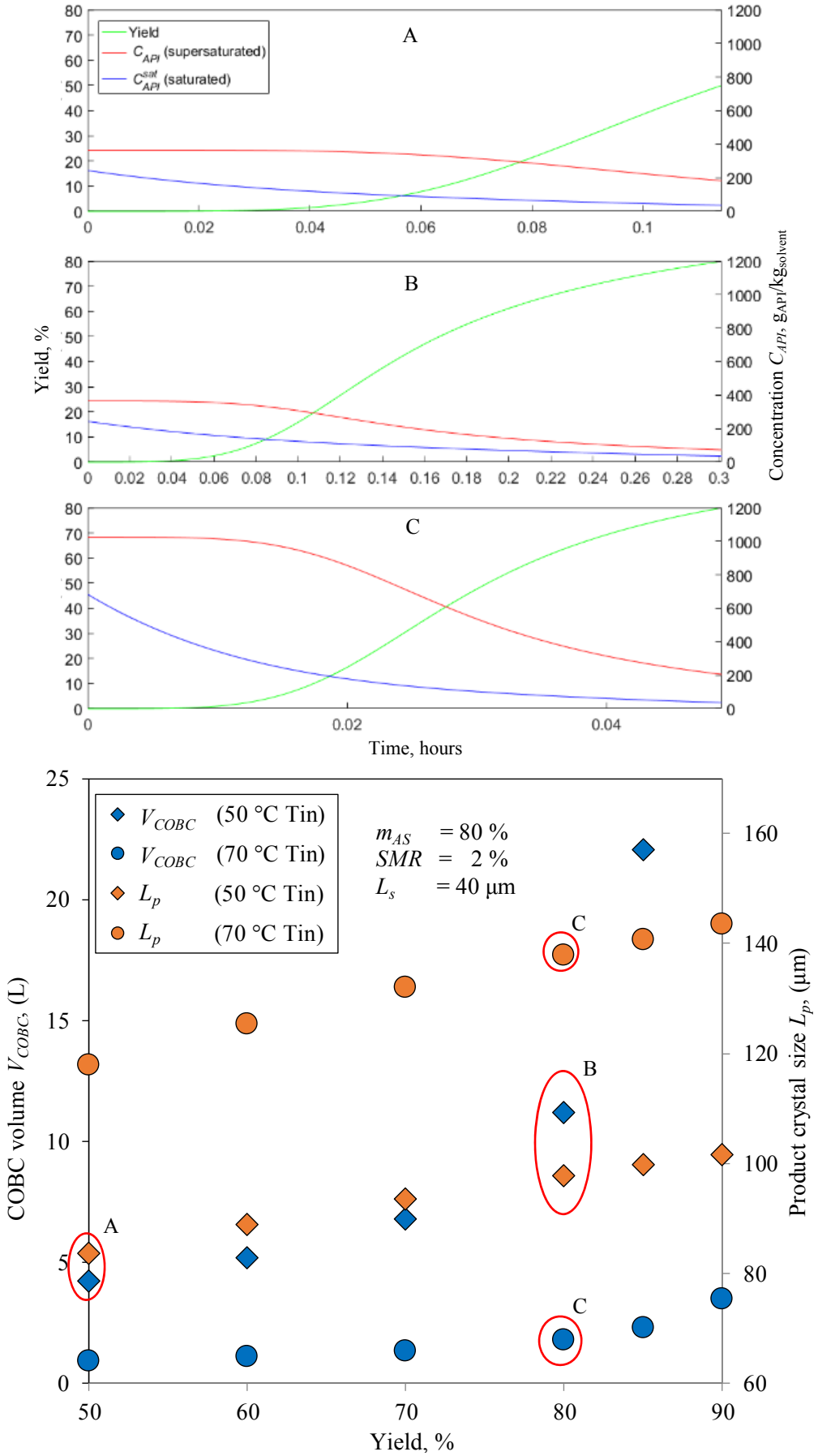

Figure 6. Trajectories of key process variables. In all cases the seed crystal size is 40 microns and the outlet temperature is 5 °C. In cases A and B, the inlet temperature is 50 °C; in case C it is 70 °C.

The estimation of the growth rate is a key aspect in this paper. The correlation used (Equation 6) has developed by Brown and Ni (Brown and Ni, 2011). Based on data acquired by visual (camera) analysis, it is applicable for crystal sizes of 43 microns and above: this was the smallest crystal size captured therein (1 pixel: 43 microns). In batch crystallisation, using seed crystals is common, because they only need be added once per batch. However, in this work, as nucleation has been considered negligible due to the conditions and the data available (e.g. Brown and Ni, 2011), the continuous addition of seed crystals has been deemed required. Because crystallisation recovers more API than is injected via seed crystals, continuous seed crystal addition can be avoided if nucleation advances at acceptably high rates; thus, investigating paracetamol nucleation kinetics will be of great benefit, to develop a crystal growth rate correlation (similar to Equation 6). Under nucleation, a key difference expected is a non-uniform crystal size, as nucleation would not occur only at the start, but throughout the crystalliser, subject to the operating conditions. The time required to achieve the desired yield, and hence the required crystalliser volume and cost, would certainly change as well.

The trajectories shown in Fig. 5 are for the case of an inlet temperature of 50 °C and seed crystal size of 40 microns, and a target yield of 50%; it corresponds to the response surfaces in Fig. 4, and the optimum is for seed mass loading of 2% and an antisolvent fraction of 80% (weight). Achieving higher yields under the same conditions becomes increasingly difficult, as illustrated in Fig. 6. The thermodynamic constraints imposed on the system (via the solubility behaviour) from using an inlet temperature of 50 °C means that compared to achieving 50% yield (Fig. 6, top trajectory) the supersaturation is very small by the time 80% yield is achieved (Fig. 6, middle trajectory). In these conditions growth rate is very low, and it takes a long time to reach the required performance (i.e. requiring a larger crystalliser as the regime is plug flow). One possible way to achieve higher yields in less time and in smaller crystallisers would be of course to operate at a higher inlet temperature (Fig. 6, bottom trajectory). With other conditions constant, a higher initial temperature allows a greater supersaturation to be maintained, achieving high yields in a reasonable time and crystalliser size.

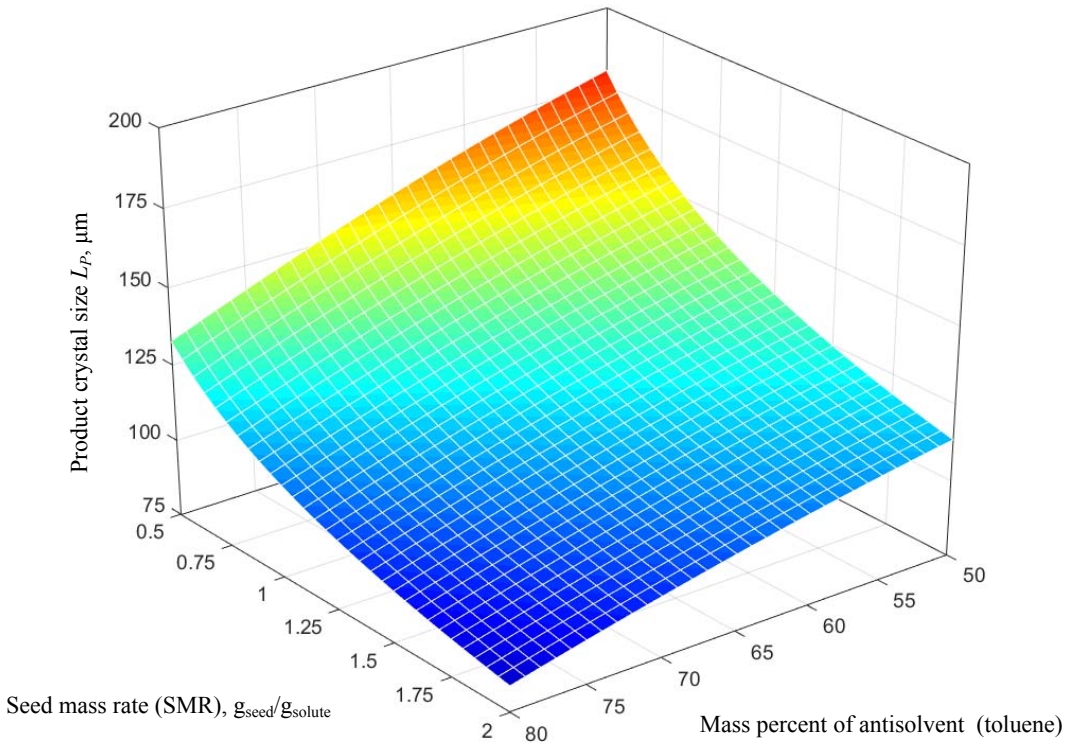

Figure 7. Product crystal size response surface for an inlet temperature of 50 °C and a seed crystal size of 40 µm.

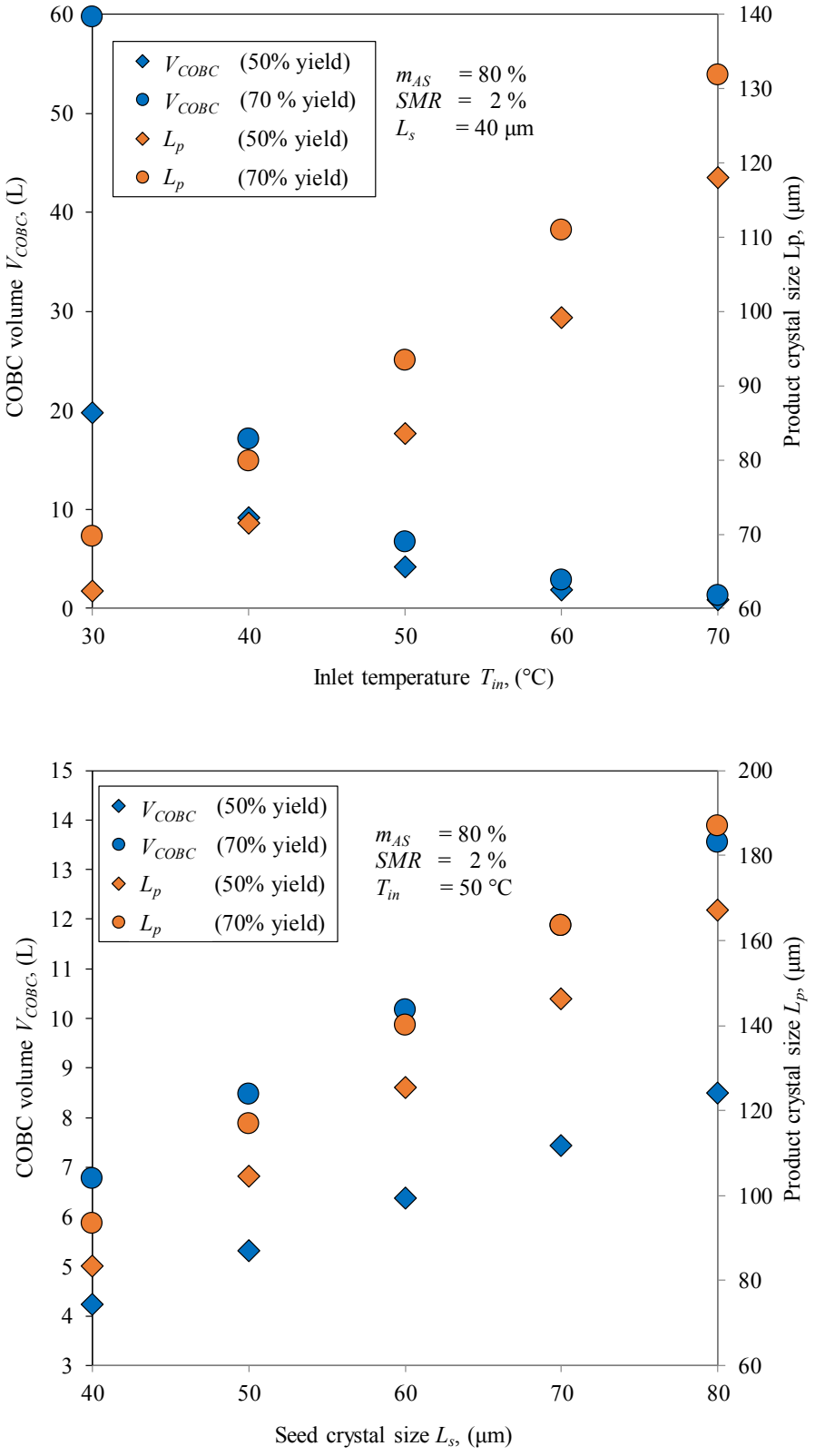

Figure 8. Variation of COBC volume and product crystal size with inlet temperature (left; constant seed crystal size) and with seed crystal size (right; constant inlet temperature).

3.2 Crystalliser volume and product crystal size

The response surface for product crystal size is given in Fig. 7. Lower antisolvent amount results in larger product crystals; again, this is an effect of seed count. With lower antisolvent amount, the mass of seed crystals added in absolute terms is less. Therefore, the seed count will lower, meaning crystals must grow more to achieve the same yield. The reason lower seed mass loading increases product size is for the same reason.

Table 1 presents how volume, residence time and product crystal size vary with seed crystal size, for the same inlet temperature of 50 °C; optima variation is less pronounced as with different inlet temperatures. Regarding the increasing product crystal size with inlet temperature (and lowering with lower inlet temperature), this makes sense, as we assume the same initial supersaturation ratio (S = 1.5, Equation 7) in all cases: the higher the inlet temperature the higher the inlet solubility, thus higher supersaturation, thus greater API content, thus greater API precipitation for the same yield, thus larger product crystal sizes (as seed count is the same).Of course, for a given seed mass loading, larger seed crystal sizes mean lower seed counts. These results are presented graphically in Fig. 8.

Also in Fig. 8 are presented values for when the target yield is 70 % (circles) instead of 50 %. As can be expected, a greater target yield leads to larger required crystalliser volumes for a given inlet temperature or seed crystal size. Also evident is the larger product crystal sizes from reaching a higher yield, which would be expected.

The change in required COBC volumes with the oscillation frequency and amplitude (Fig. 9) produce a clear trend of lower volumes; this is to be expected, as higher ω increases Re_o, which increases growth rates. The variation of volumes and product crystal sizes for different required target yields (other results presented in this work are for yields of 50 %) is also illustrated in Fig. 6; again, the inlet temperature is 50 °C and the seed crystal size is 40 microns. The product crystal size increases fairly linearly. In contrast, the required crystal volumes exponentially increase, and indeed

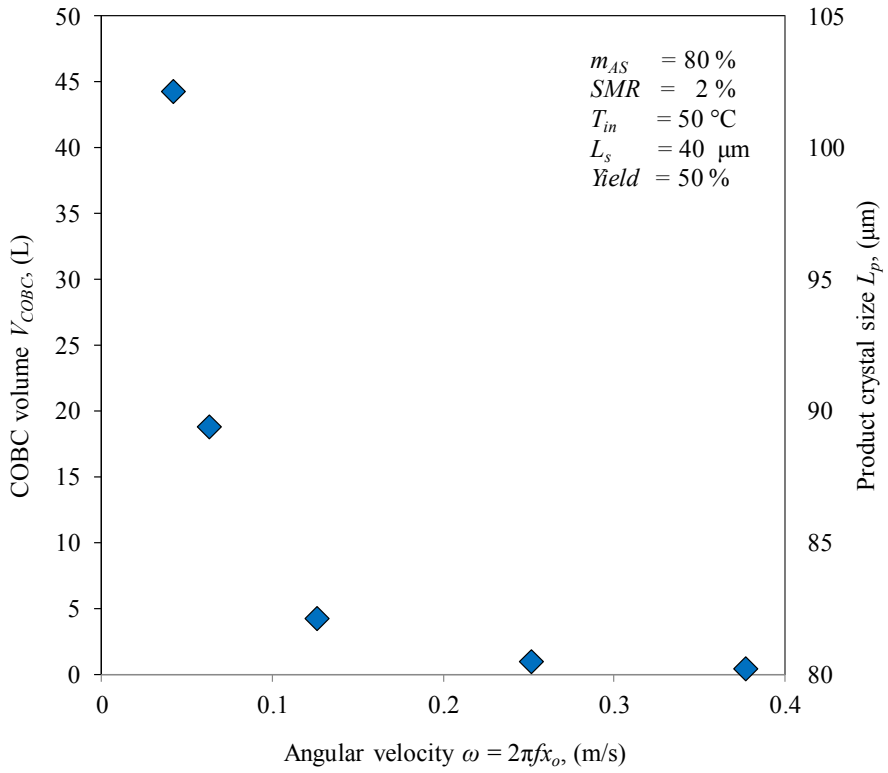

Figure 9. Variation of COBC volume with angular velocity of the oscillatory fluid motion (left) and variation of COBC volume and product crystal size with different crystallisation yield targets (right). In both cases there is constant inlet temperature (50 °C) and seed crystal size (40 microns).

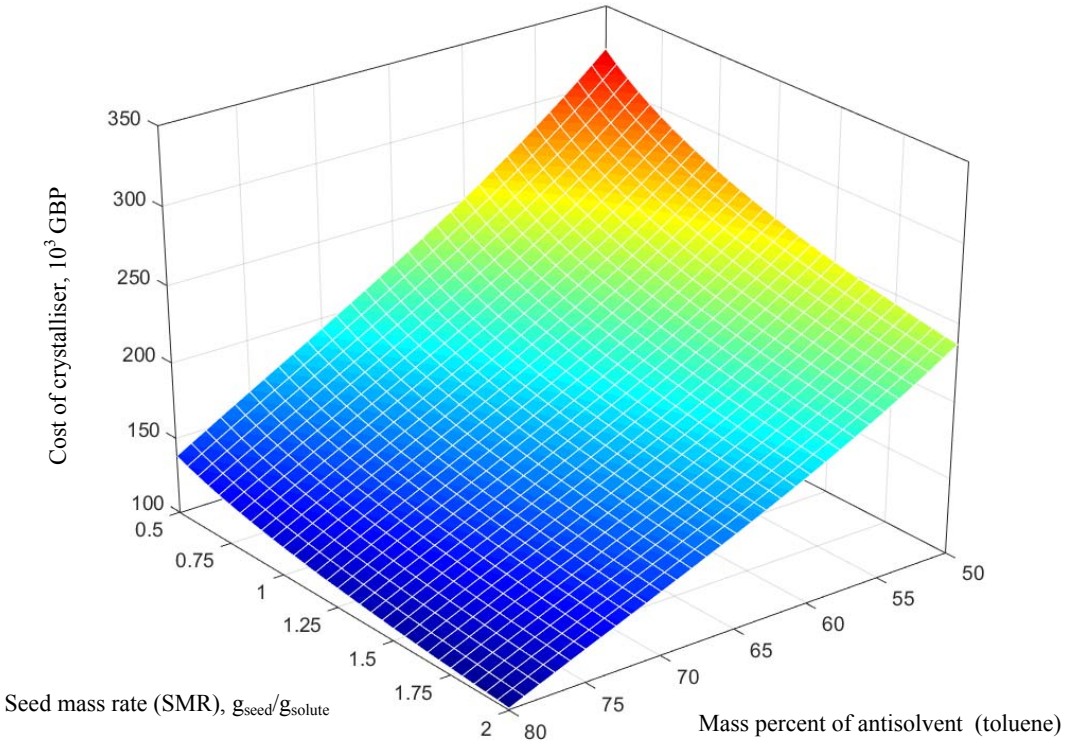

Figure 10. Total cost response surface for an inlet temperature of 50 °C and a seed crystal size of 40 microns

achieving 90% yield is impractical (under the given conditions; as previously discussed, differing operating temperatures for example can make higher yields achievable).

3.3 Crystalliser cost

Given a desired yield of 50 %, the total cost response surface for an inlet temperature of 50 °C and a seed crystal size of 40 microns is given in Fig. 10. The optimal solution (cost = 101,370 GBP) is pushed to bounds. It is evident that the rate of antisolvent use affects the total cost more significantly than the seed mass loading. Greater rates of antisolvent use result in lower costs via lower required residence times, due to faster growth rates. The tabulated values (Table 1) illustrate how the optimum changes with varying inlet temperatures, with a constant seed crystal size of 40 microns. Increasing the inlet temperature can drastically lower the cost via small required volumes and residence times.

Crystalliser cost here is defined as the Capital Expenditure, calculated from a power-law relationship with crystalliser volume (Equation 1). More detailed design and cost estimations could include a more explicit relation between unit operation design and cost, as well as the inclusion of additional sources of cost contributing to the Capital Expenditure (such as installation costs) or the inclusion of Operating Expenditure (which could indeed be expected to vary with size, capacity and operation). However, as the process being evaluated here is a single crystallisation operation on its own, with no upstream or downstream operations, inclusion of additional cost detail as described above is complicated. In essence, what is performed here is an evaluation of how a variables such as inlet temperature, target yield, and seed crystal size affect the required crystalliser volumes, with the cost calculated as another way to visualise the response of the crystalliser volumes.

3.4 Material efficiency (E-factor)

The E-factor, first used by Sheldon (2012), is a versatile and useful Green Chemistry metric. The simplest definition the E-factor is the quantity of waste generated per unit of product, in mass terms.

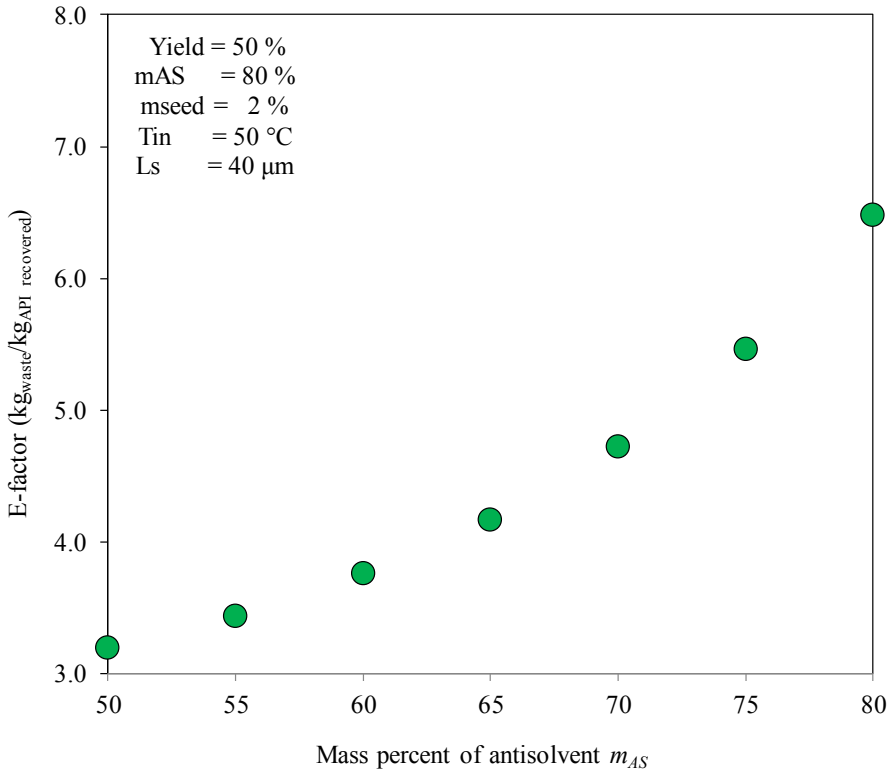

Figure 11. Variation in attained E-factor with increasing rates of antisolvent use (mass percent of the fluid which is antisolvent).

Values as high as 200 for the E-factor are not uncommon for pharmaceutical process, which are invariably batch operations; this in contrast to those highly efficient industries which very heavily rely on continuous production techniques, such as the oil and gas sector, which have representative E-factors in the order of 0.1, indicating significantly less amounts of relative waste amounts (Ritter, 2013). In this work, the E-factor is computed where the product is (pure) recovered API, while the waste consists of waste solvent and antisolvent and unrecovered API. Evaluating E-factors (Fig. 11), we can see that for a given yield they worsen with increasing antisolvent quantity; E-factor is invariant with seed mass loading. However, with worsening E-factor, costs improve, highlighting the frequently conflicting requirements in process design and evaluation.

4 CONCLUSIONS

The solved optimisation cases illustrate the benefits and drawbacks of different combinations of solvent and antisolvent, in both technical and sustainability terms, and the varying impacts of inlet temperature, seed mass loading, seed crystal size, mechanical operation of the crystalliser, and rate of antisolvent use. For a desired yield of 50%, the latter has the most significant effect on crystalliser cost (Capital Expenditure), while seed mass loading also has a strong effect. Higher required yields require exponentially larger and costlier crystallisers. Paracetamol nucleation and growth kinetics can be readily incorporated in the model presented. The tradeoff between material efficiency (or E-factor), COBC volume and cost underscores the competing objectives frequently arising in process design.

ACKNOWLEDGEMENTS
The authors gratefully acknowledge the financial support of the Engineering and Physical Sciences Research Council (EPSRC) via a Doctoral Training Partnership (DTP) studentship awarded to Mr H.G. Jolliffe. Moreover, Dr D.I. Gerogiorgis acknowledges a Royal Academy of Engineering (RAEng) Industrial Fellowship. Tabulated and cited literature data suffice for reproduction of all original process simulation and optimisation results, and no other supporting data are required to ensure reproducibility.

5 NOMENCLATURE

a	Cost coefficient for crystalliser cost estimation via Equation (1), GBP
a_{osc}	Amplitude of oscillation, m
ASR	Mass fraction of antisolvent (balance is process solvent)
B	Nucleation rate, s^{-1}
C_{API}	API solute concentration, g cm^{-3}
ΔC_{API}	Degree of supersaturation, g cm^{-3}
C_{API}^{sat}	Saturation API solute concentration, g cm^{-3}
d	Internal diameter of the Continuous Oscillatory Baffled Crystalliser, m
f_{osc}	Frequency of oscillation, Hz
G	Growth rate, m s^{-1}
k_v	Volume shape factor
L	Size (length) of crystals, m
L_p	Size (length) of product crystals, m
L_s	Size (length) of seed crystals, m
m	Exponent in Equation (1)
m_{AS}	Mass percent of antisolvent (balance is process solvent)
n	Number of crystals
$\dot{Q}_{AS}$	rate of antisolvent addition, mL min^{-1}
$\dot{Q}_{Tot}$	Volumetric flowrate, Ls^{-1}
Re_n	Net flow Reynolds Number
Re_o	oscillatory flow Reynold Number
r_o	Radius of nucleating crystal, m
S	Supersaturation ratio
SMR	Seed mass rate
T	Temperature, K
T_{in}	Inlet temperature, K
t	Time, s
u_{net}	Bulk fluid superficial velocity, m s^{-1}
V_{COBC}	Crystalliser volume, L
μ_j	jth moment
μ_{mix}	Bulk fluid viscosity, Pa s
ρ_{API}	Crystal density, g cm^{-3}
ρ_{mix}	Fluid bulk density, kg m^{-3}
τ_{req}	Required residence time, s
ψ	Ratio of Re_o and Re_n
ω	Oscillatory flow angular velocity, m s^{-1}

6 REFERENCES

Abejón, R., Garea, A., Irabien, A., 2014. Analysis and optimization of continuous organic solvent nanofiltration by membrane cascade for pharmaceutical separation. *AIChE J.* 60, 931–948. doi:10.1002/aic.14345

Baxendale, I.R., Braatz, R.D., Hodnett, B.K., Jensen, K.F., Johnson, M.D., Sharratt, P., Sherlock, J.-P., Florence, A.J., 2015. Achieving continuous manufacturing: technologies and approaches for synthesis, workup, and isolation of drug substance. *J. Pharm. Sci.* 104, 781–791. doi:10.1002/jps.24252

Biegler, L.T., Grossmann, I.E., 2004. Retrospective on optimization. *Comput. Chem. Eng.* 28, 1169–1192. doi:10.1016/j.compchemeng.2003.11.003

Bogdan, A.R., Poe, S.L., Kubis, D.C., Broadwater, S.J., McQuade, D.T., 2009. The continuous-flow synthesis of ibuprofen. *Angew. Chem. Int. Ed.* 48, 8547–8550. doi:10.1002/anie.200903055

Boukouvala, F., Ierapetritou, M.G., 2013. Surrogate-based optimization of expensive flowsheet modeling for continuous pharmaceutical manufacturing. *J. Pharm. Innov.* 8, 131–145. doi:10.1007/s12247-013-9154-1

Brown, C.J., Lee, Y.C., Nagy, Z.K., Ni, X., 2014. Evaluation of crystallization kinetics of adipic acid in an oscillatory baffled crystallizer. *Cryst. Eng. Comm.* 16, 8008–8014. doi:10.1039/C4CE00192C

Brown, C.J., Ni, X., 2011. Online evaluation of paracetamol antisolvent crystallization growth rate with video imaging in an oscillatory baffled crystallizer. *Cryst. Growth Des.* 11, 719–725. doi:10.1021/cg1011988

EFPIA, 2013. The Pharmaceutical Industry in Figures - Key Data 2013 [WWW Document]. URL http://www.efpia.eu/uploads/Figures_Key_Data_2013.pdf (accessed 1.31.14).

Escotet-Espinoza, M.S., Rogers, A., Ierapetritou, M., 2016. Optimization methodologies for the production of pharmaceutical products, in: Ierapetritou, M.G., Ramachandran, R. (Eds.), *Process Simulation and Data Modeling in Solid Oral Drug Development and Manufacture: Methods in Pharmacology and Toxicology*. Springer, New York, pp. 281–309. doi:10.1007/978-1-4939-2996-2_9

Gernaey, K.V., Cervera-Padrell, A.E., Woodley, J.M., 2012. A perspective on PSE in pharmaceutical process development and innovation. *Comput. Chem. Eng.* 42, 15–29. doi:10.1016/j.compchemeng.2012.02.022

Gerogiorgis, D.I., Barton, P.I., 2009. Steady-state optimization of a continuous pharmaceutical process, *Comput.-Aided Chem. Eng.*, 27, 927–932.

Grom, M., Stavber, G., Drnovšek, P., Likozar, B., 2016. Modelling chemical kinetics of a complex reaction network of active pharmaceutical ingredient (API) synthesis with process optimization for benzazepine heterocyclic compound. *Chem. Eng. J.* 283, 703–716. doi:10.1016/j.cej.2015.08.008

Heider, P.L., Born, S.C., Basak, S., Benyahia, B., Lakerveld, R., Zhang, H., Hogan, R., Buchbinder, L., Wolfe, A., Mascia, S., Evans, J.M.B., Jamison, T.F., Jensen, K.F., 2014. Development of a multi-step synthesis and workup sequence for an integrated, continuous manufacturing process of a pharmaceutical. *Org. Process Res. Dev.* 18, 402–409. doi:10.1021/op400294z

Hodges, P., 2015. Bayer Technology Services purchases NiTech DN15 Continuous Crystalliser [WWW Document]. NiTech Solutions. URL http://www.nitechsolutions.co.uk/bayer-technology-services-purchases-nitech-dn15-continuous-crystalliser/ (accessed 11.9.17).

Hopkin, M.D., Baxendale, I.R., Ley, S.V., 2010. A flow-based synthesis of Imatinib: the API of Gleevec. *Chem. Commun.* 46, 2450–2452. doi:10.1039/C001550D

Jolliffe, H.G., Gerogiorgis, D.I., 2015. Continuous pharmaceutical process engineering and economics: Investigating technical efficiency, environmental impact and economic viability. *Chim. Oggi–Chem. Today* 33(6), 29-32.

Jolliffe, H.G., Gerogiorgis, D.I., 2017. Technoeconomic optimization of a conceptual flowsheet for continuous separation of an analgaesic Active Pharmaceutical Ingredient (API). *Ind. Eng. Chem. Res.* 56, 4357–4376. doi:10.1021/acs.iecr.6b02146

Jolliffe, H.G., Gerogiorgis, D.I., 2017. Technoeconomic optimisation and comparative environmental impact evaluation of continuous crystallisation and antisolvent selection for artemisinin recovery. *Comput. Chem. Eng.* 103, 218–232. doi: 10.1016/j.compchemeng.2017.02.046

Kwon, J.S.I., Nayhouse, M., Christofides, P.D., Orkoulas G., 2014a. Modeling and control of crystal shape in continuous protein crystalization, *Chem. Eng. Sci.*, 107, 47–57. doi: 10.1016/j.ces.2013.12.005

Kwon, J.S.I., Nayhouse, M., Orkoulas G., Christofides, P.D., 2014b. Crystal shape and size control using a plug flow crystallization configuration, *Chem. Eng. Sci.*, 119, 30–39. doi:10.1016/j.ces.2014.07.058

Kwon, J.S.I., Nayhouse, M., Orkoulas G., Christofides, P.D., 2014c. Enhancing the crystal production rate and reducing polydispersity in continuous protein crystallization, *Ind. Eng. Chem. Res.*, 53(40), 15538–15548. doi: 10.1021/ie5008163

Lawton, S., Steele, G., Shering, P., Zhao, L., Laird, I., Ni, X.-W., 2009. Continuous crystallization of pharmaceuticals using a continuous oscillatory baffled crystallizer. *Org. Process Res. Dev.* 13, 1357–1363. doi:10.1021/op900237x

McGlone, T., Briggs, N.E.B., Clark, C.A., Brown, C.J., Sefcik, J., Florence, A.J., 2015. Oscillatory Flow Reactors (OFRs) for continuous manufacturing and crystallization. *Org. Process Res. Dev.* 19, 1186–1202. doi:10.1021/acs.oprd.5b00225

Ott, D., Borukhova, S., Hessel, V., 2016. Life cycle assessment of multi-step rufinamide synthesis – from isolated reactions in batch to continuous microreactor networks. *Green Chem.* 18, 1096–1116. doi:10.1039/C5GC01932J

Ott, D., Kralisch, D., Denčić, I., Hessel, V., Laribi, Y., Perrichon, P.D., Berguerand, C., Kiwi-Minsker, L., Loeb, P., 2014. Life cycle analysis within pharmaceutical process optimization and intensification: case study of active pharmaceutical ingredient production. *Chem. Sus. Chem.* 7, 3521–3533. doi:10.1002/cssc.201402313

Patel, M.P., Shah, N., Ashe, R., 2011. Robust optimisation methodology for the process synthesis of continuous technologies, *Comput.-Aided Chem. Eng.* 29, 351–355.

Rogers, A., Ierapetritou, M., 2015. Challenges and opportunities in modeling pharmaceutical manufacturing processes. *Comput. Chem. Eng.*, 81, 32–39. doi:10.1016/j.compchemeng.2015.03.018

Rogers, A.J., Inamdar, C., Ierapetritou, M.G., 2014. An integrated approach to simulation of pharmaceutical processes for solid drug manufacture. *Ind. Eng. Chem. Res.* 53, 5128–5147. doi:10.1021/ie401344a

Sato, H., Watanabe, S., Takeda, D., Yano, S., Doki, N., Yokota, M., Shimizu, K., 2015. Optimization of a crystallization process for orantinib active pharmaceutical ingredient by design of experiment to control residual solvent amount and particle size distribution. *Org. Process Res. Dev.* 19, 1655–1661. doi:10.1021/acs.oprd.5b00149

Sen, M., Rogers, A., Singh, R., Chaudhury, A., John, J., Ierapetritou, M.G., Ramachandran, R., 2013. Flowsheet optimization of an integrated continuous purification-processing pharmaceutical manufacturing operation. *Chem. Eng. Sci.* 102, 56–66. doi:10.1016/j.ces.2013.07.035

Shi, D., El-Farra, N.H., Li, M., Mhaskar, P., Christofides, P.D., 2006. Predictive control of particle size distribution in particulate processes, *Chem. Eng. Sci.*, 61, 268–281. doi: 10.1016/j.ces.2004.12.059

Sudha, C., Srinivasan, K., 2013. Supersaturation dependent nucleation control and separation of mono, ortho and unstable polymorphs of paracetamol by swift cooling crystallization technique. *Cryst. Eng. Comm.* 15, 1914–1921. doi:10.1039/C2CE26681D